Available online at www.sciencedirect.com
ScienceDirect
Journal of Magnetic Resonance 188 (2007) 68–73
JMR Journal of Magnetic Resonance
www.elsevier.com/locate/jmr

Single loop multi-gap resonator for whole body EPR imaging of mice at 1.2 GHz

Sergey Petryakov, Alexandre Samouilov, Eric Kesselring, Tomasz Wasowicz, George L. Caia, Jay L. Zweier *

Center for Biomedical EPR Spectroscopy and Imaging, Davis Heart and Lung Research Institute, Division of Cardiovascular Medicine, Department of Internal Medicine, The Ohio State University, Columbus, OH 43210, USA

Received 8 February 2007; revised 13 April 2007
Available online 9 June 2007

Abstract

For whole body EPR imaging of small animals, typically low frequencies of 250–750 MHz have been used due to the microwave losses at higher frequencies and the challenges in designing suitable resonators to accommodate these large lossy samples. However, low microwave frequency limits the obtainable sensitivity. L-band frequencies can provide higher sensitivity, and have been commonly used for localized in vivo EPR spectroscopy. Therefore, it would be highly desirable to develop an L-band microwave resonator suitable for in vivo whole body EPR imaging of small animals such as living mice. A 1.2 GHz 16-gap resonator with inner diameter of 42 mm and 48 mm length was designed and constructed for whole body EPR imaging of small animals. The resonator has good field homogeneity and stability to animal-induced motional noise. Resonator stability was achieved with electrical and mechanical design utilizing a fixed position double coupling loop of novel geometry, thus minimizing the number of moving parts. Using this resonator, high quality EPR images of lossy phantoms and living mice were obtained. This design provides good sensitivity, ease of sample access, excellent stability and uniform B_1 field homogeneity for in vivo whole body EPR imaging of mice at 1.2 GHz.

Keywords: Electron paramagnetic resonance; Imaging; Spectroscopy; Resonator

1. Introduction

For in vivo EPR spectroscopy and imaging applications, it is of critical importance to maximize sensitivity. Recently, systems have been developed to enable combined EPR/NMR co-imaging to provide anatomical mapping of free radicals in living animals [1,2]. For these applications, it is essential to maximize both system sensitivity and stability. For small animal EPR imaging, typically low frequencies have been used such as 300 MHz [3–6]. However, the selection of low microwave frequency limits the obtainable sensitivity [7–11]. With increasing frequency, microwave power absorption and consequent sample heating increases, and microwave tissue penetration depth falls. Therefore, in vivo whole body EPR imaging measurements in small animals such as rats and mice have typically been limited to frequencies of 300 and 750 MHz, respectively. L-band frequencies, around 1.2 GHz, have been commonly used for localized in vivo EPR spectroscopy in small animals and high quality microwave bridges and microwave components are available. Therefore, it would be highly desirable to develop an L-band microwave resonator suitable for in vivo whole body EPR imaging in small animals such as living mice.

Design and construction of an L-band volume resonator large enough to accommodate a living mouse is highly challenging considering the requirements for RF field homogeneity. Since living animals are lossy samples that

* Corresponding author. Fax: +614 247 7845.
E-mail address: jay.zweier@osumc.edu (J.L. Zweier).

1090-7807/$ - see front matter © 2007 Elsevier Inc. All rights reserved.
doi:10.1016/j.jmr.2007.05.021

heavily load the resonator, the resonator design requires special coupling and high loaded Q characteristics [12–15]. Several articles have reported RF resonators that can provide sufficient space for living animals in EPR spectroscopy and imaging [16–20], however, these resonators have been designed for lower frequencies.

We describe the development of a single loop multi-gap (SLMG) resonator design with provisions for EPR/NMR co-imaging applications in small animals. This development focused on maximization of B_1 field homogeneity and minimization of E field over the sample volume. In addition, to facilitate in vivo applications on these small animals, there was a special effort to maximize the mechanical stability of the resonator and also achieve high coupling efficiency. These goals were achieved by a highly segmented 16-gap loop-gap structure with novel coupling mechanism design that eliminated moving parts. This design provides ease of sample access, excellent stability and good performance for in vivo whole body EPR spectroscopy and imaging of mice at 1.2 GHz.

1.1. Construction of the resonator

There is a size limitation for conventional loop-gap resonators as the length of the loop should be small compared with one quarter wavelength ($\lambda/4$) [21,22]. For a given loop diameter, if the number of capacitive gaps is increased N-fold the resonance frequency increases by the $\sqrt{N}$ [23].

Dimensions of loop-gap resonators are characteristically 1/10–1/4 of the wavelength [21]. Consequently, for a frequency of about 1.2 GHz and diameter of 42 mm and length 48 mm, at least eight gaps are necessary. However, EPR imaging experiments with living animals demand good homogeneity of the B_1 field, therefore a 16-gap design of the loop-gap resonator was selected. The biggest challenge in EPR experiments with living animals is to overcome motion-induced noise. The electric field is mainly responsible for loss within lossy animal tissue, so it should be minimized within the sample area.

Therefore, we designed and constructed a loop-gap resonator with 16 gaps oriented radially from the center. This design concept has previously been shown to provide good spatial separation of E and B_1 fields [14]. In the reported resonator design, the maximum B_1 field is concentrated at the center of resonator and maximum E field is concentrated away from the sample near the outer shield. The best separation of RF field components was obtained by using gaps oriented in a radial pattern from the sample as shown in Fig. 1. This configuration provided better loading capability and higher loaded Q than other resonator designs [21,22]. Thus, increasing the number of gaps allows constructing a relatively large full-body volume resonator for 1.2 GHz. Spatial distribution of the RF electric and magnetic field components allows us to present the resonator as a lumped circuit device with inductances and capacitances connected serially [24]. The equation for the resonator frequency is as follows:

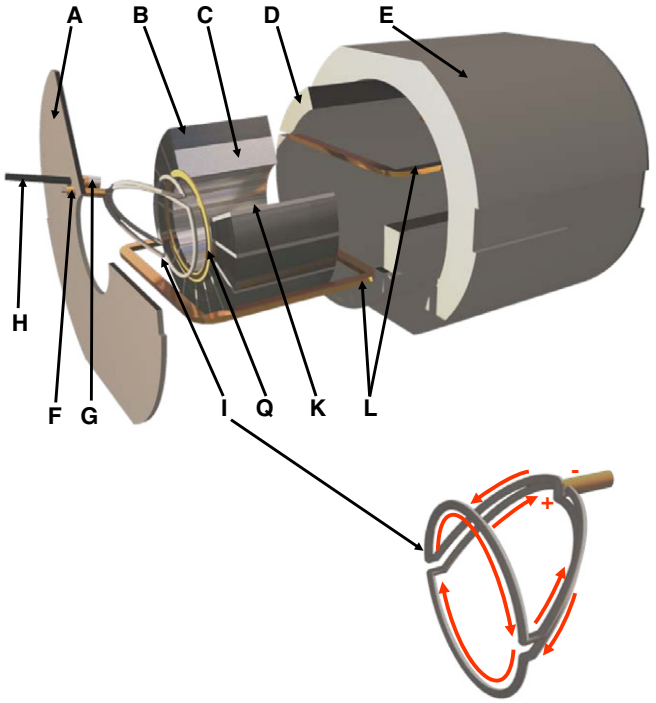

Fig. 1. Detailed mechanical layout of the single loop multi-gap resonator with 16 gaps. Combination of expanded and cut off views. (A) Front lid (rear lid is not shown); (B) Segment of the resonator; (C) Silver plated part of the segment; (D) PVC reinforcing inner shell; (E) Housing; (F) RF cable; (G) Coupling capacitor; (H) Coupling control rod; (I) Double coupling loop. Coupling loop also shown separately, enlarged and from different perspective in order to clarify its 3D structure. Arrows show current paths; (Q) Reinforcing ring/separator; (K) Resonator gap; (L) Modulation coils.

$$\omega = 1/\sqrt{L_{\text{sum}} C_{\text{sum}}}, \quad \text{where} \tag{1}$$

$$L_{\text{sum}} = L * N; \tag{2}$$

L – inductance of the individual loop,
C – capacitance of the individual gap,
N – number of gaps.
Since $C_{\text{sum}} = C/N$ and $C = \varepsilon_o S_c/d$, where
ε_o – dielectric constant of the plastic in the gap,
S_C – area of the capacitive plates,
d – thickness of the resonator gaps,

this allows us to estimate the physical parameters of the resonator, the area and the thickness of the resonator gaps. However, the increased number of resonator gaps should cause deterioration of the quality factor of the empty resonator, according to $Q = i\omega L/R$, where R is the resistance of one section of the resonator [25]. If one considers only resistive loss in the conductors, Q will drop because of the decrease of the resonator inductance. This inductance, L, can be approximated by application of the equation for inductance for a solenoid with fractional number of turns $n = 1/N$ (1, 1/2, 1/4 etc.):

$$L = k\mu(4\pi n^2 S_L/l), \quad \text{where} \tag{3}$$

k – coefficient considering diameter and length, l of the solenoid,
S_L – area of the solenoid cross-section.

Therefore, with the increase in number of gaps, Q will be approximately inversely proportional to $\sqrt{N}$. However, this generalized approach is relevant to the lumped schematic representation of the resonator and extrapolating it to continuous element design adds restrictions to its applicability. The dimensions of the resonator were chosen in order to accommodate and obtain EPR images of the whole body of a living mouse, which requires at least ~30 mm diameter. This resonator was designed with EPR/NMR co-imaging experiments in mind, with ability of the resonators to slide over the fixed sample utilizing a special stage, providing a method to maintain alignment between gradients and sample while exchanging EPR or NMR resonators over the sample [25]. Special provisions for EPR/NMR co-imaging with requisite sliding mechanism require support for the sample holder, therefore the inner diameter of the resonator had to be increased to 42 mm. Increasing the inner diameter of the loop-gap resonator reduces the filling factor and compromises its sensitivity [26,27]. However, considering the dielectric loss of living tissues, increased distance from the capacitive plates will improve the Q factor of the loaded resonator, resonator loading capability, homogeneity in the sample volume, and attenuate motion-induced noise. The resonator (Fig. 2) was built for EPR/NMR co-imaging experiments, and this design also allows stand-alone use for conventional EPR spectroscopy and imaging applications.

The development of the resonator focused on the following critical areas: (1) maximization of the B_1 homogeneity of the resonator; (2) maximization of its mechanical stability and suppression of motion-induced noise; and (3) provision for highly efficient and readily adjustable coupling to allow maximum loading with highly lossy biological samples.

2. Mechanical design

Mechanical stability of the resonator plays an important role in achieving good signal-to-noise ratio with live animal experiments and can be significantly improved by constructing the resonator without moving parts and with increased weight. As seen in Fig. 1, the resonator body is constructed from 16 Rexolite segments [3] assembled in a cylindrical structure with a 42 mm i.d., 88 mm o.d., and 48 mm length. The segments are separated by sixteen 1.68 mm thick polystyrene plates (K). Before final assembly, to form the conductive resonator surfaces, silver was electro-sprayed on the inner faces of the segments and 13 mm portion of each side of the prism (C) (Fig. 1). The assembled structure was pressed into a hollow cylinder (D) made of PVC plastic and formed a single, structurally

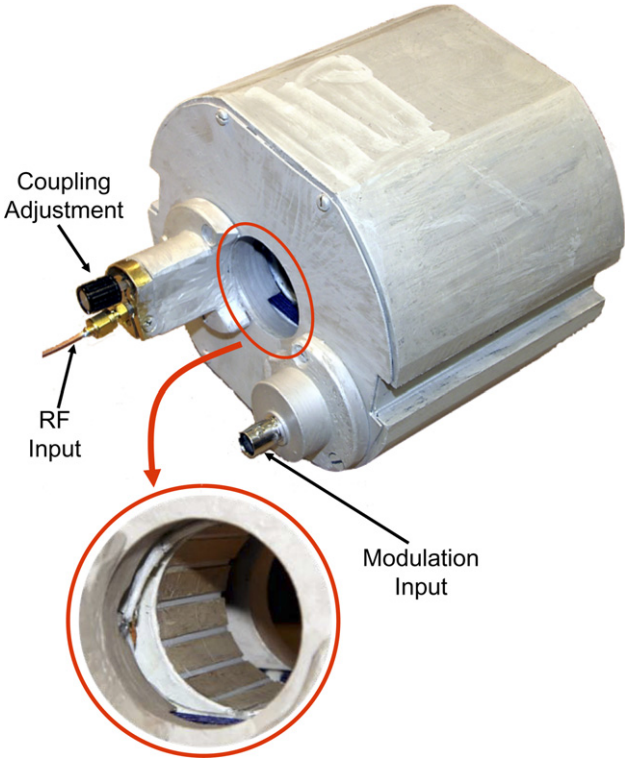

Fig. 2. A photo of the single loop multi-gap resonator setup. Resonator is shown positioned inside the shield.

solid unit. The cylinder is painted with conductive paint and thus, serves as an electrical shield. The cylinder has two slots which create a form for the modulation coils (L). The resonator is magnetically coupled using a segmented loop (I) with feeding leads displaced laterally to preserve sample access. In order to increase rigidity, the coupling loop (I) was attached to a polystyrene ring (Q) which simultaneously serves as a spacer between the loop and the resonator. The polystyrene ring was also attached to the resonator. The coupling capacitor (G) is soldered directly to the feeding cable (F), and its tuning rod (H) extends through the holes in the nylon cylinder and the lid. The outside surface of the resonator case and its edge surfaces are painted with the conductive silver paint which forms an additional electrical shield. This nylon cylinder, together with the resonator and the form-wound modulation coils, fit into the nylon case (E). The nylon case has two parallel slots which allow the resonator to slide over the sample [28]. The resonator housing is equipped with two silver plated polystyrene lids (A), which not only mechanically protect the resonator and coupling mechanism, but also serve as an electrical shield.

3. Electrical design of the resonator and its coupling mechanism

Adjustable inductive coupling has been widely used in many loop-gap resonators since it provides a wide range of coupling and allows uniform "feeding" of all resonator

loops. With this configuration, the coupling loop is usually positioned between the resonator and the shield. The inherent weakness of this approach is that any change in the relative position of these elements causes alterations in the resonator frequency and coupling to the feeding cable, which amplifies motion-induced noise. However, implementing electrical capacitive coupling, which is free from the above drawback for the multi-loop/gap resonator design is difficult, since parallel feeding of all gaps is impossible due to space limitations. An alternating, every other, feed of gaps will reduce the number of feeders but compromise homogeneity. Therefore, a modified coupling loop design was implemented for this resonator. In order to reduce or eliminate mechanically-induced noise, the copper wire coupling loop was "reinforced" with a rigid plastic ring and firmly attached to the resonator body. There are two possible approaches to achieve variable coupling: varying the mutual inductance between the coupling loop and the resonator, and varying the inductance of the coupling loop. Both approaches were used. Initial coupling was achieved by altering spacing ring thickness. Additional coupling adjustment was provided by a serially connected capacitor. As for the resonator, there are limitations on the size of the coupling loop. For efficient coupling, the circumference of the coupling loop can not be longer than $\lambda/2$ of the wavelength in the conductor. So, in order to provide homogeneous coupling for L-band frequencies [29,30], it should be no more than 63 mm (or 20 mm in diameter). To overcome these limitations, a parallel double loop design was implemented. In order to provide open access to the resonator, the loop, together with $\lambda/4$ long feeding lines was transformed into a 3D symmetrical structure with feeding leads laterally displaced (Fig. 1I). The symmetrical structure and mutually inverted connection to the feeding cable makes it insensitive to the magnetic fields perpendicular to the plane of the coils. This is essential for reduction of DC offset of the signal induced by the field modulation. Additional attenuation of the modulation induced offset is achieved by the coupling capacitor, serially connected to the RF cable, which serves as high pass filter.

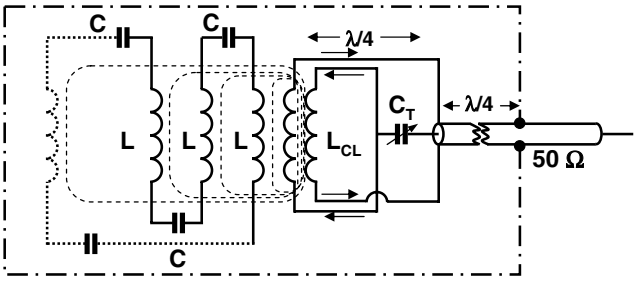

Fig. 3. Lumped element presentation of the schematic diagram of the resonator. C, Capacitance of the individual gap; L, inductance of the individual loop; L_{CL}, inductance of the coupling loop; C_T, adjustable tuning capacitor. Arrows indicate the direction of the current in the coupling loop.

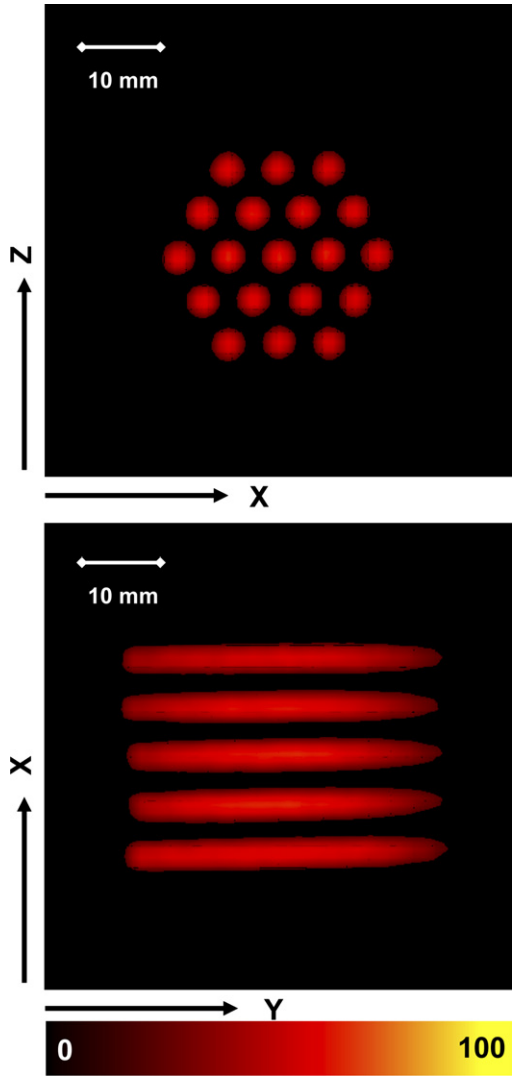

Fig. 4. Middle slices of the 3D EPR image of the phantom consisting of 19 plastic tubes filled with 1 mM TAM used for RF field homogeneity assessment. The parameters used for the EPRI acquisition were as follows: frequency 1.19 GHz, microwave power ~300 mW, modulation amplitude 0.012 mT at 100 kHz, field gradient 0.5 mT/cm, scan time 5.2 s, 36×36 projections, field of view 6 cm, scan width 3 mT.

Table 1
Microwave parameters of the 16-gap resonator

Diameter (mm)	Length (mm)	f_0 EPR empty (GHz)	f_0 EPR with sample++ (GHz)	Q^a EPR with 11 cc load*	Q^a EPR with 20 cc load**
42	48	1.22	1.216	72	57

*Sample, 11 cc of aqueous 0.45% saline solution.
**Sample, 20 cc of aqueous 0.45% saline solution.
[a] Q-factor was measured with network analyzer Agilent 8719 ES [19].

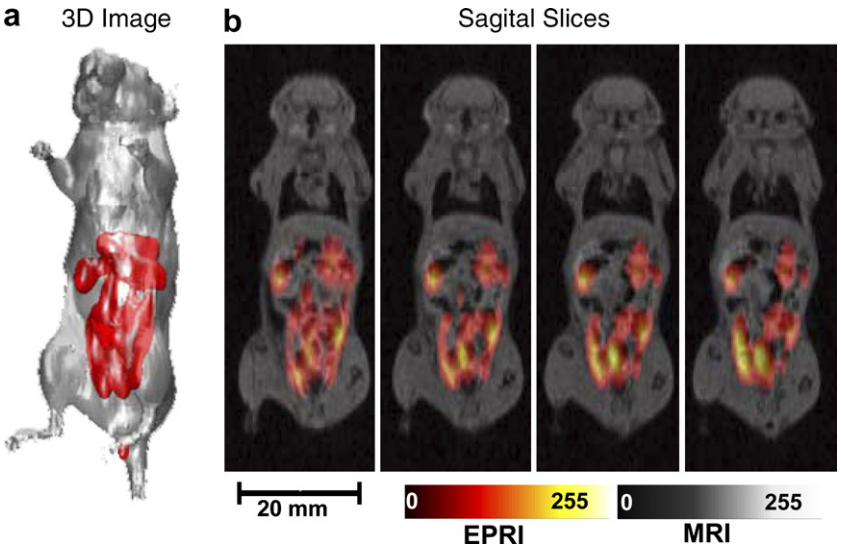

Fig. 5. EPR image of a live mouse fed with paramagnetic activated carbon. (a) Surface rendering of the 3D EPR image superimposed with 3D rendering of the NMR image. (b) XY slices from the same 3D image. EPR images rendered in color superimposed with corresponding slices of NMR image rendered in gray scale. The parameters used for the EPRI acquisition were as follows: frequency 1.19 GHz, scan width 6.0 mT, microwave power ~300 mW, modulation amplitude 0.1 mT, maximum field gradient 1.5 mT/cm along X and Z directions, and 0.6 mT/cm along Y, scan time 2.6 s, 32×32 projections. The MRI data was acquired at 0.38 T magnetic field, using gradient echo pulse sequence with the following parameters: 12.5 kHz bandwidth, matrix $128 \times 128 \times 128$, repetition time TR = 70 ms, echo delay time TE = 10 ms, number of excitations (NEX) = 1, field of view (FOV) in plane 40×40 mm, FOV in slice direction 100 mm (transverse slice thickness of 0.78 mm), flip angle 65°.

Equivalent schematics of the resonator (Fig. 3) illustrate that the coupling loops are coupled with the entire magnetic flux of the resonator. Parallel coupling loops are phased in a manner that each individual loop adds magnetic flux; however, RF currents are completely compensated in the feeding lines. Also this "opposite" connection of feeding lines makes them insensitive to the RF irradiation in the planes, parallel to the axis of the resonator. However, to ensure that the coupling loop efficiently radiates in the plane perpendicular to the resonator, the resonator assembly had to be shielded in the axial direction. All resonator loops are serially connected through the gaps, presented as capacitors. By themselves they are partially coupled with each other and the coupling loop, and connected in parallel towards the magnetic flux.

4. Results

Coupling of the resonator was efficient and easily adjusted for a broad range of in vitro and in vivo experiments with sample volume up to 22 cc 0.45% saline or 25 g mouse (Table 1). In order to check the B_1 field homogeneity of the resonator, a phantom was constructed consisting of polystyrene plastic tubes diameter 4 mm, arranged in a circular pattern and filled to a height of 11 mm with a solution of 1 mM tetrathiatriarylmethyl radical (TAM) [31]. A series of 2D and 3D images were acquired [32]. The uniform intensity of the images confirms the good B_1 homogeneity of the resonator along all axies (Fig. 4). As expected, the resonator showed a small resonant frequency shift of <20 MHz during coupling adjustment that was within the tuning mode range of the microwave bridge and did not adversely effect overall ease of coupling adjustment. Good stability was observed in these studies enabling continued imaging for periods of up to 3 h. After initial set up with suitable coupling of the resonator and tuning of the bridge, little further adjustment was needed during live animal experiments and the EPR resonant frequency remained within the AFC range of the bridge. The resonator demonstrated good sensitivity, and good quality images were obtained with phantoms filled with 1 mM solution of TAM and with a live mouse fed with paramagnetic activated charcoal to enable EPR imaging of the GI tract (Figs. 4 and 5).

5. Summary and conclusion

An improved 1.2 GHz 16-gap resonator with inner diameter of 43 mm and length of 48 mm was designed and constructed for whole body EPR imaging of small living animals. The resonator has improved field homogeneity and stability to animal-induced motional noise. The stability of the resonator was achieved with electrical and mechanical design utilizing fixed positioned double coupling loop of novel geometry, thus minimizing the number of moving parts. This design provides good sensitivity, ease of sample access, excellent stability and good B_1 field homogeneity for in vivo whole body EPR spectroscopy and imaging of mice at 1.2 GHz.

Acknowledgment

This work was supported by NIH Research Grants EB0890 and EB4900. We thank Dr. Yuanmu Deng for the help in image reconstructions.

References

[1] Y. Kawada, H. Hirata, H. Fujii, Use of multi-coil parallel-gap resonators for co-registration EPR/NMR imaging, J. Magn. Reson. 184 (1) (2007) 29–38.

[2] G. He, Y. Deng, H. Li, P. Kuppusamy, J.L. Zweier, EPR/NMR co-imaging for anatomic registration of free-radical images, Magn. Reson. Med. 47 (3) (2002) 571–578.

[3] M. Ono, A. Suenaga, H. Hirata, Experimental investigation of RF magnetic field homogeneity in a bridged loop-gap resonator, Magn. Reson. Med. 47 (2) (2002) 415–419.

[4] B.B. Williams, H. al Hallaq, G.V. Chandramouli, E.D. Barth, J.N. Rivers, M. Lewis, V.E. Galtsev, G.S. Karczmar, H.J. Halpern, Imaging spin probe distribution in the tumor of a living mouse with 250 MHz EPR: correlation with BOLD MRI, Magn. Reson. Med. 47 (4) (2002) 634–638.

[5] M.A. Foster, I.A. Grigor'ev, D.J. Lurie, V.V. Khramtsov, S. McCallum, I. Panagiotelis, J.M. Hutchison, A. Koptioug, I. Nicholson, In vivo detection of a pH-sensitive nitroxide in the rat stomach by low-field ESR-based techniques, Magn. Reson. Med. 49 (3) (2003) 558–567.

[6] S. Subramanian, K. Matsumoto, J.B. Mitchell, M.C. Krishna, Radio frequency continuous-wave and time-domain EPR imaging and Overhauser-enhanced magnetic resonance imaging of small animals: instrumental developments and comparison of relative merits for functional imaging, NMR Biomed. 17 (5) (2004) 263–294.

[7] G.A. Rinard, R.W. Quine, S.S. Eaton, G.R. Eaton, Frequency dependence of EPR signal intensity, 250 MHz to 9.1 GHz, J. Magn. Reson. 156 (1) (2002) 113–121.

[8] G.A. Rinard, R.W. Quine, S.S. Eaton, G.R. Eaton, Frequency dependence of EPR signal intensity, 248 MHz to 1.4 GHz, J. Magn. Reson. 154 (1) (2002) 80–84.

[9] G.R. Eaton, S.S. Eaton, G.A. Rinard, Frequency dependence of EPR sensitivity, in: P. Blumler, B. Blumich, R. Botto, E. Fukushima (Eds.), Spatially Resolved Magnetic Resonance, Wiley-VCH, Weinheim, 1998.

[10] Y.E. Nesmelov, A. Gopinath, D.D. Thomas, Aqueous sample in an EPR cavity: sensitivity considerations, J. Magn. Reson. 167 (1) (2004) 138–146.

[11] Y.S. Lebedev, High-frequency continuous wave electron spin resonance, in: L. Kevan, N.K. Bowman (Eds.), Modern Pulsed and Continuous-Wave Electron Spin Resonance, Wiley, New York, 1990, p. 372.

[12] P. Fajer, D. Marsh, Microwave field inhomogeneities and the effect of cavity Q in saturation transfer ESR spectra. Dependence on sample size, J. Magn. Reson. 49 (1982) 212–224.

[13] P. Wojciech, F. Wojciech, Field distributions in loop-gap resonators, Meas. Sci. Technol. 4 (1993) 1363–1369.

[14] J.L. Zweier, P. Kuppusamy, Electron paramagnetic resonance measurements of free radicals in the intact beating heart: a technique for detection and characterization of free radicals in whole biological tissues, Proc. Natl. Acad. Sci. USA 85 (15) (1988) 5703–5707.

[15] G.A. Rinard, R.W. Quine, S.S. Eaton, G.R. Eaton, Microwave coupling structures for spectroscopy, J. Magn. Reson. A105 (1993) 137–144.

[16] R. Diodato, M. Alecci, J.A. Brivati, V. Varoli, A. Sotgiu, Optimization of axial RF field distribution in low-frequency EPR loop-gap resonators, Phys. Med. Biol. 44 (5) (1999) N69–N75.

[17] J.A. Brivati, A.D. Stevens, A radiofrequency ESR spectrometer for in vivo imaging, J. Magn. Reson. 92 (1991) 480–489.

[18] K. Oikawa, T. Ogata, H. Togashi, H. Yokoyama, H. Ohya-Nishiguchi, H. Kamada, A 3D- and 4D-ESR imaging system for small animals, Appl. Radiat. Isotopes 47 (11-12) (1996) 1605–1609.

[19] K.H. Ahn, V.S. Subramanian, C. Mailer, X. Pan, H.J. Halpern, Scaling of EPR spectra-spatial images: Images of samples greater than 5 cm in linear dimension, Denver, Colorado, USA, 2005, p 45.

[20] M. Alecci, I. Seimenis, S.J. McCallum, D.J. Lurie, M.A. Foster, Nitroxide free radical clearance in the live rat monitored by radio-frequency CW-EPR and PEDRI, Phys. Med. Biol. 43 (7) (1998) 1899–1905.

[21] J.S. Hyde, W. Froncisz, Loop-gap resonators, in: M.C.R. Symons (Ed.), Electron Spin Resonance. Specialist Periodical Reports, vol. 10, The Royal Society of Chemistry, 1986, pp. 175–184.

[22] J.S. Hyde, W. Froncisz, Loop gap resonators, in: A.J. Hoff (Ed.), Advanced EPR: Applications in Biology and Biochemistry, Elsevier, Amsterdam, 1989, pp. 277–306.

[23] A. Mehdizadeh, An Investigation on Electromagnetic Fields and Properties of the Loop-Gap Resonator, a Lumped Mode Microwave Resonant Structure, Ph.D. Thesis. Milwaukee, Wisconsine: Marquette University, 1983.

[24] Y.D. Shirman, Moscow, Makvis, 1998 (in Russian). Electronic Systems Construction Foundations and Theory Handbook. Makvis, Moscow, 1998, pp 250–252.

[25] G.L. Matthaei, L.E. Young, M.T. Jones, Microwave Filters, Impedance-Matching Networks, and Coupling Structures: Mcgraw-Hill Book Company.

[26] J.L. Zweier, P. Kuppusamy, EPR spectroscopy of free radicals in the perfused heart, Curr. Top. Biophys. 18 (1994) 14–25.

[27] J.L. Zweier, P. Kuppusamy, Study of free radicals in the intact beating heart using low frequency electron paramagnetic resonance spectroscopy, Phys. Med. 7 (1991) 29–37.

[28] A. Samouilov, G.L. Caia, E. Kesselring , S. Petryakov, T. Wasowicz, J.L. Zweier, Development of a hybrid EPR/NMR co-imaging system. Magn. Reson. Med., in press.

[29] H. Hirata, T. Walczak, H.M. Swartz, Electronically tunable surface-coil-type resonator for L-band EPR spectroscopy, J. Magn. Reson. 142 (1) (2000) 159–167.

[30] H. Hirata, T. Walczak, H.M. Swartz, Characteristics of an electronically tunable surface-coil-type resonator for L-band electron paramagnetic resonance spectroscopy, Rev. Sci. Instrum. 72 (2001) 2839–2841.

[31] S. Xia, F.A. Villamena, C.M. Hadad, P. Kuppusamy, Y. Li, H. Zhu, J.L. Zweier, Reactivity of Molecular oxygen with ethoxycarbonyl derivatives of tetrathiatriarylmethyl radicals, J. Org. Chem. 71 (2006) 7268–7279.

[32] G. He, S.P. Evalappan, H. Hirata, Y. Deng, S. Petryakov, P. Kuppusamy, J.L. Zweier, Mapping of the B1 field distribution of a surface coil resonator using EPR imaging, Magn. Reson. Med. 48 (6) (2002) 1057–1062.